

3.1 Introduction

In this chapter the major features of the prompt radiation fields produced by electrons are described. It includes an extensive discussion of the electromagnetic cascade and of the shielding of photoneutrons and high energy particles that result from these interactions. The utilization of Monte Carlo calculations in electron shielding problems is also addressed. The material presented in this chapter is useful for understanding electron, photon and photoneutron radiation from electron accelerators used in medicine and in high energy research. As has been pointed out by Silari et al. (Si99) it is also useful in understanding the radiation that may be produced by some accelerator components, such as superconducting RF cavities, even when operated apart from the main accelerator.

3.2. Unshielded Radiation Produced by Electron Beams

At all energies photons produced by **bremsstrahlung** dominate the unshielded radiation field aside from the hazard of the direct beam. As the energy increases, neutrons become a significant problem. For $E_o > 100$ MeV, the **electromagnetic cascade** must be considered and will be discussed later in this chapter. A useful rule of thumb is that electrons have a finite range in any material proportional to the initial kinetic energy of the electron, E_o , (MeV):

For $2 < E_o < 10$ MeV,

$$R = 0.6E_o \text{ (g cm}^{-2}\text{)}. \quad (3.1)$$

In air over this energy domain, R (meters) $\approx 5 E_o$ (MeV). Above an energy of 10 MeV or so, dependent upon the absorbing medium, the loss of energy begins to be dominated by **radiative** processes, whereby photons are emitted begin to dominate over those losses of energy due to collisions. This will be discussed further in Section 3.2.2.

3.2.1 Dose Equivalent Rate in a Direct Beam of Electrons

At any accelerator, the dose equivalent rate in the direct particle beam is general larger than at any other point. This is certainly true at electron accelerators. Swanson (Sw79a) has given a "conservative" rule of thumb for electrons in the energy domain of $1 < E_o < 100$ MeV:

$$\frac{dH}{dt} = 1.6 \times 10^{-4} \phi, \quad (3.2)$$

where dH/dt is the dose equivalent rate (rem h^{-1}) and ϕ is the flux density ($\text{cm}^{-2} \text{s}^{-1}$). One of the problems at the end of this chapter examines the domain of validity of this approximation. The coefficient is 1.6×10^{-6} if dH/dt is to be in Sv h^{-1} with ϕ remaining in units of $\text{cm}^{-2} \text{s}^{-1}$.

3.2.2 Bremsstrahlung

Bremsstrahlung is the radiative energy loss of electrons as they interact with materials. It appears in the form of photons. An important parameter when considering the radiative energy loss of electrons in matter is the **critical energy**, E_c . The critical energy is the energy above which the radiative losses of energy exceed that due to ionization for electrons. For electrons, the value of E_c is a smooth function of atomic number;

$$E_c = \frac{800 \text{ (MeV)}}{Z + 1.2}, \quad (3.3a)$$

where Z is the atomic number of the material. For muons in solid materials (PDG96) (see Section 1.4.1) the corresponding critical energy, $E_{c,muon}$, is much larger;

$$E_{c,muon} = \frac{6590 \text{ GeV}}{(Z + 2.17)^{0.885}}. \quad (3.3b)$$

The transition from dominance by ionization to dominance by radiation is a smooth one. The stopping power for electron or muons may be written as the sum of collisional and radiative components, respectively:

$$\left(\frac{dE}{dx}\right)_{tot} = \left(\frac{dE}{dx}\right)_{coll} + \left(\frac{dE}{dx}\right)_{rad} \quad (3.4)$$

Another parameter of significant importance is the **radiation length**, X_0 , which is the mean thickness of material over which a high energy electron loses all but $1/e$ of its energy by bremsstrahlung. This parameter is the approximate scale length for describing high-energy electromagnetic cascades, supplanting the ionization range for even moderate electron energies. It also plays a role in the "scaling" of multiple scattering for all charged particles and was discussed in Section 1.4.2. The radiation length is approximated by Eq. (1.21). It turns out for high energy electrons that the rate of radiative energy loss is given by

$$\left(\frac{dE}{dx}\right)_{rad} = -\frac{E}{X_0}, \quad (3.5)$$

so that under these conditions (i.e., where loss by ionization can be neglected), the energy of the electron, E , as a function of thickness of shield penetrated, x , is given by

$$E(x) = E_0 e^{-x/X_0}, \quad (3.6)$$

where the energy of the incident particle is E_0 and x and X_0 are in the same units.

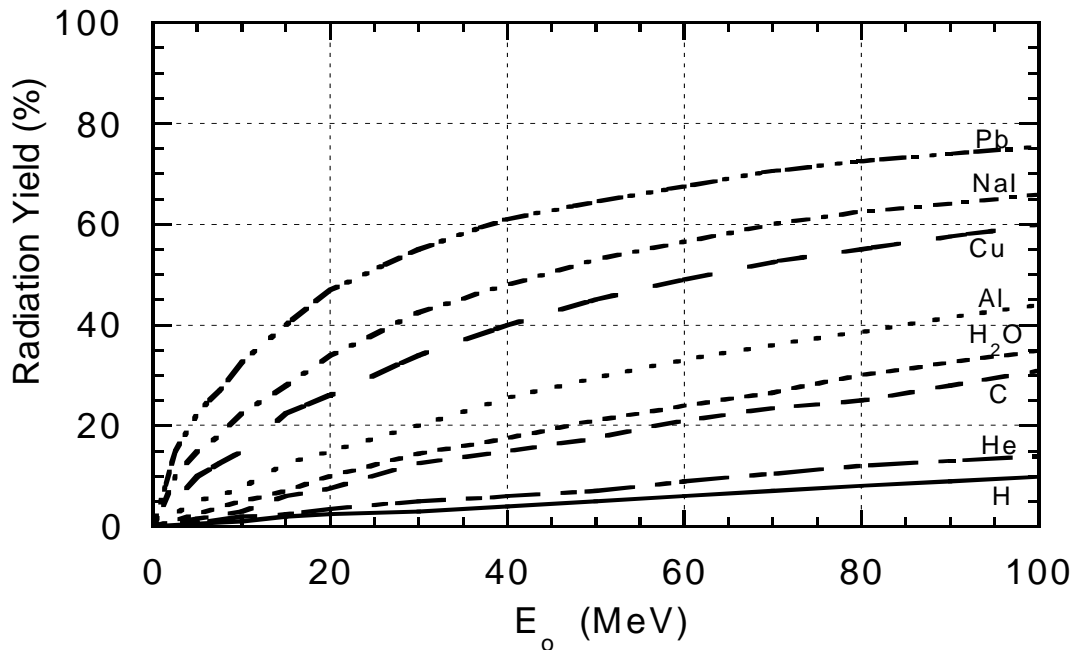


Fig. 3.1 Bremsstrahlung efficiency for electrons stopped in various materials. This is the fraction (in per cent) of the kinetic energy of incident electrons converted to radiation as a function of incident energy E_o . The remainder of the kinetic energy is transferred to the medium by ionization. [Adapted from (Sw79a)].

Figure 3.1 gives the percentage of energy E_o that appears as radiation for various materials as a function of energy. External bremsstrahlung develops as a function of target thickness and is described by a **transition** curve. As the thickness increases, the intensity of the radiation increases until re-absorption begins to take effect. Then, self-shielding begins to take over. One talks about the maximum as a "thick-target" bremsstrahlung spectrum. This phenomenon becomes dominant above energies of about 100 MeV for low-Z materials and above 10 MeV for high-Z materials.

The energy spectrum of the radiated photons ranges from zero to the energy of the incident electron and the number of photons in a given energy interval is approximately inversely proportional to the photon energy. The amount of energy radiated per energy interval is practically constant according to Schopper et al. (Sc90). Detailed spectral information for bremsstrahlung photons have been provided by various workers. Figures 3.2 and 3.3 are provided as examples of such spectra at moderate electron beam energies.

For thin targets ($X \ll X_o$), the spectrum of photons of energy k per energy interval dk , dN/dk , can be approximated by:

$$\frac{dN}{dk} \approx \frac{X}{X_o k}. \quad (3.7)$$

Thick targets require consideration of the electromagnetic cascade. In general, the spectra fall as $1/k^2$ at $\theta = 0$ and even faster at larger angles (Sw79a).

A more detailed parameterization of the normalized total photon differential yield per incident electron, $dN/d\Omega$, for photons of all energies has been reported by Swanson and Thomas (Sw90), with improvements suggested by Nelson (Ne97):

$$\frac{1}{E_o} \frac{dN}{d\Omega} = 4.76 E_o \exp(-\theta^{0.6}) + 1.08 \exp(\theta/72) \text{ (photons sr}^{-1} \text{ GeV}^{-1} \text{ electron}^{-1}\text{)}. \quad (3.8)$$

This expression is normalized to results involving iron and copper targets at $E_o = 15$ GeV. In Eq. (3.8), E_o is in GeV and θ is in degrees.

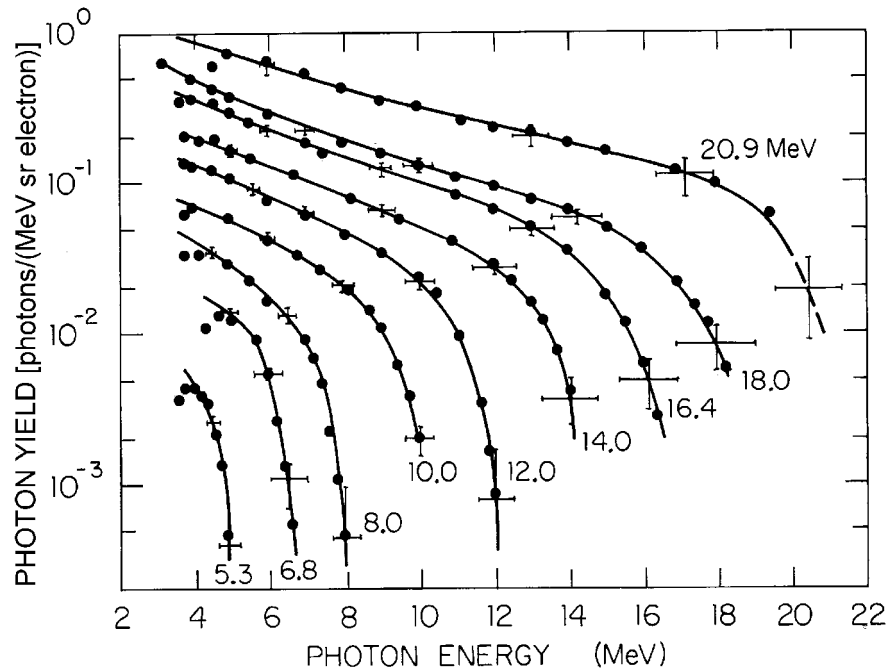


Fig. 3.2 Bremsstrahlung spectra measured at zero degrees from intermediate thickness ($0.2 X_o$) targets of high atomic number (Z) material. The data points are measurements of O'Dell et al. (OD68) [adapted by Swanson (Sw79a)].

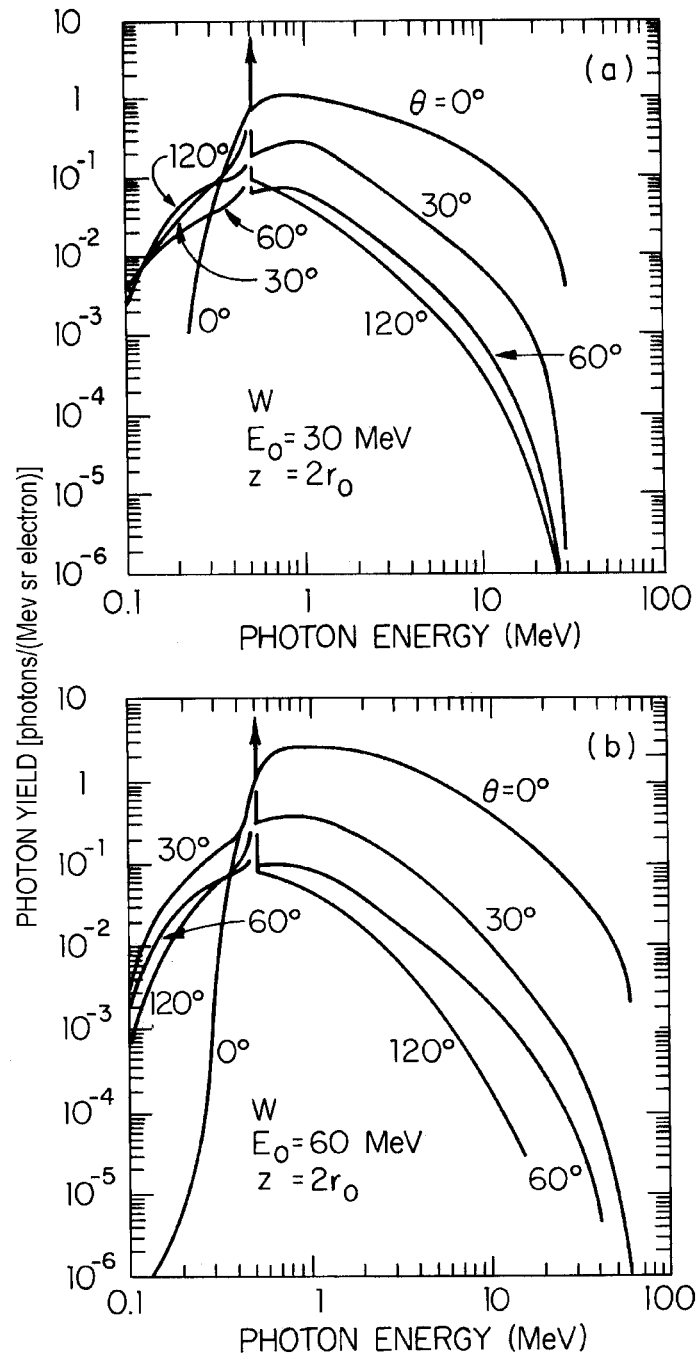


Fig. 3.3 Spectra of bremsstrahlung photons emerging in various directions from thick tungsten targets irradiated by normally incident monoenergetic electron beams at two different energies. The target thickness at both energies is twice the mean electron ionization range, r_0 , given by the continuous slowing down approximation. The arrows indicate the abundant positron annihilation radiation at 0.511 keV. **a)** Kinetic energy 30 MeV, thickness = 24 g cm^{-2} ($3.6 X_0$); **b)** 60 MeV, thickness = 33 g cm^{-2} ($4.9 X_0$). [Adapted from Berger and Seltzer (Be70) by Swanson (Sw79a).]

Swanson has developed three "rules of thumb" which parameterize this behavior for the absorbed dose rates, dD/dt , normalized to one kW of incident beam power for E_o in MeV, expected at one meter from a point "target" (Sw79a) :

Swanson's Rule of Thumb 1:

$$\frac{dD}{dt} \approx 20E_0^2 \text{ (Gy m}^2\text{)(kW}^{-1} \text{ h}^{-1}\text{)} \text{ at } \theta = 0^\circ, E_o < 15 \text{ MeV.} \quad (3.9)$$

Swanson's Rule of Thumb 2:

$$\frac{dD}{dt} \approx 300E_o \text{ (Gy m}^2\text{)(kW}^{-1} \text{ h}^{-1}\text{)} \text{ at } \theta = 0^\circ, E_o > 15 \text{ MeV.} \quad (3.10)$$

Swanson's Rule of Thumb 3:

$$\frac{dD}{dt} \approx 50 \text{ (Gy m}^2\text{)(kW}^{-1} \text{ h}^{-1}\text{)} \text{ at } \theta = 90^\circ, E_o > 100 \text{ MeV.} \quad (3.11)$$

One can scale these results to other distances (in meters) by using the inverse square law.

Figure 3.4 shows the behavior for a high-Z target. It should be noted that higher absorbed dose rates at 90° can arise in certain circumstances due to the presence of softer radiation components. The forward intensity is a slowly varying function of target material except at very low Z.

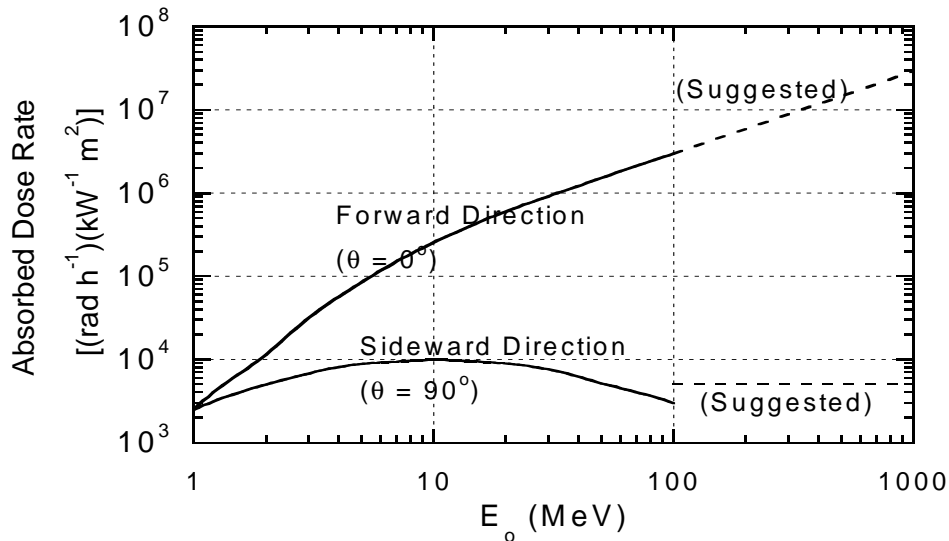


Fig. 3.4 Thick target bremsstrahlung from a high atomic number target. Absorbed dose rates at 1 meter per unit incident electron beam power (kW) are given as a function of incident electron energy E_o . The dashed lines represent a reasonable extrapolation of the measured values. The dose rates measured in the sideward direction (smoothed for this figure) depend strongly on target and detector geometry and can vary by more than a factor of two. The dashed line at 90° represents the more penetrating radiation component to be considered in room shielding. [Adapted from (Sw79a).]

The angular full width, $\theta_{1/2}$, of the forward lobe (at half-intensity) is approximately given by a relation due to Swanson (Sw79a),

$$E_o \theta_{1/2} = 100 \text{ (MeV degrees)}. \quad (3.12)$$

Alternatively, according to Schopper et al. (Sc90) the average angle of emission is of the order of m_e/E_o (radians) where m_e is the rest mass (in energy units, e.g., MeV) of the electron.

At higher energies ($E_o > \text{approximately } 100 \text{ MeV}$), the electromagnetic cascade development in accelerator components is very important and can result in a forward "spike" of photons with a characteristic angle of $\theta_c = 29.28/E_o$ (degrees, if E_o is in MeV). At $\theta = \theta_c$ the intensity of the spike has fallen to $1/e$ of its value at $\theta = 0$.

3.2.3 Synchrotron Radiation

Swanson (Sw90) presents a summary discussion of this important phenomenon. The movement of electrons in a circular orbit results in their centripetal acceleration. This gives rise to emission of photons. At nonrelativistic energies, this radiation is largely isotropic. However, for relativistic energies, a condition readily achievable for accelerated electron beams, the photons emerge in a tight bundle along a tangent to any point on a circular orbit. Figure 3.5 shows this bundle. The characteristic angle (i.e., the angle of $1/e$ of the zero degree intensity) of this "lobe" is

$$\theta_c = \frac{1}{\gamma} = \sqrt{1 - \beta^2} \text{ radians}. \quad (3.13)$$

The median energy of the power spectrum, ϵ_c , is given in terms of the total energy, W (GeV), and bending radius, R (meters) by

$$\epsilon_c = \frac{2.218W^3}{R} \text{ (keV)}. \quad (3.14)$$

For singly-charged particles of other masses, m_p , one should multiply this energy by a factor of $(m_e/m_p)^3$. The radiated power, P , for a circulating electron current, I (milliamperes) is,

$$P = \frac{88.46W^4 I}{R} \text{ (watts)}. \quad (3.15)$$

For singly-charged particles of other masses, m_p , one should multiply this power by a factor of $(m_e/m_p)^4$. More details on this subject, including the details of the angular distributions and spectra of the emitted photons, have been given in detail by Jackson (Ja75) with a good summary provided by the Particle Data Group (PDG96). Fig. 3.6 gives the universal radiation spectrum for high energies.

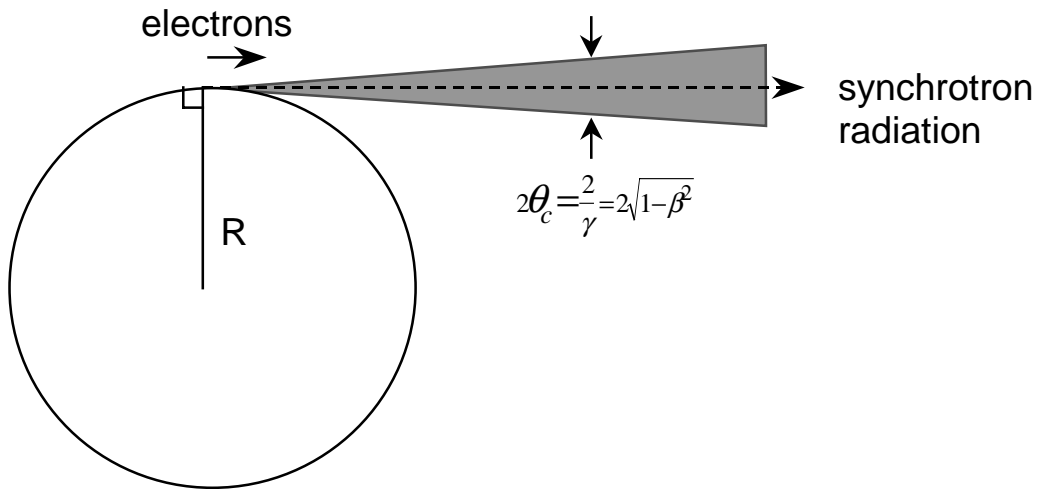


Fig. 3.5 Synchrotron radiation pattern for relativistic particles at the instantaneous location denoted by "electrons". Twice the opening angle, θ_c , is shown as the shaded region.

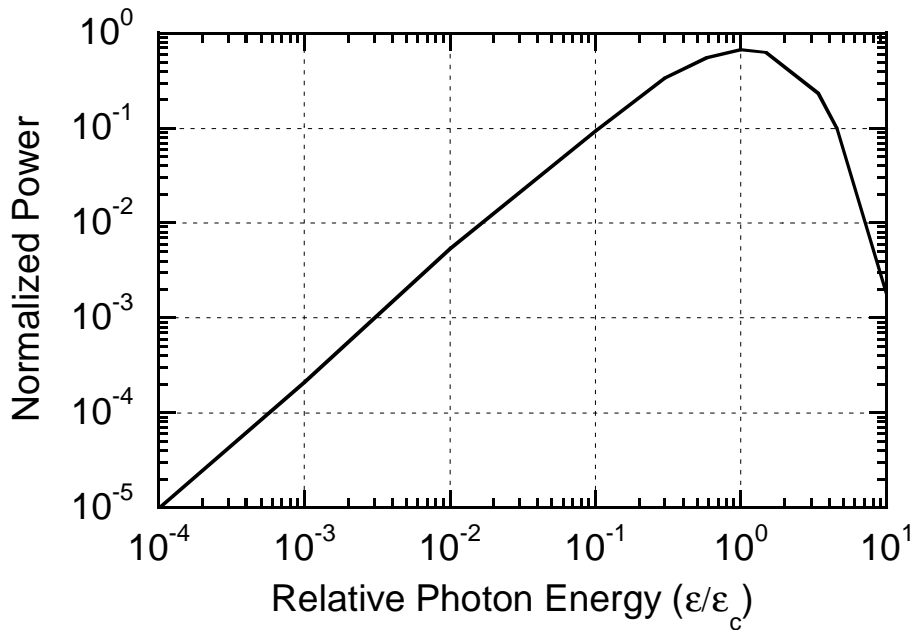


Fig. 3.6 Universal synchrotron radiation spectrum. The graph gives the relative power as a function of photon energy in units of characteristic energy, ϵ_c . This spectrum yields unity if integrated over all energies. [Adapted from (Sw90).]

3.2.4 Neutrons

3.2.4.1 *Giant Photonuclear Resonance Neutrons*

Neutron production can be expected to occur in any material irradiated by electrons in which bremsstrahlung photons above the material-dependent threshold are produced. This threshold varies from 10 to 19 MeV for light nuclei and 4 to 6 MeV for heavy nuclei. Thresholds of 2.23 MeV for deuterium and 1.67 MeV for beryllium are noteworthy exceptions. Between this threshold and approximately 30 MeV, a production mechanism known as the **giant photonuclear resonance** is the most important source of neutron emission from material. Swanson (Sw79a) has given a detailed description of this process that is summarized here. A simple picture of this phenomenon is that the electric field of the photon produced by bremsstrahlung transfers its energy to the nucleus by inducing an oscillation in which the protons as a group move oppositely to the neutrons as a group. This process has a broad maximum cross section at photon energies, k_o , between about 20-23 MeV for light nuclei for materials having mass numbers A less than about 40. For heavier targets, the peak is at an energy of approximately $k_o = 80A^{-1/3}$. Schopper et al. (Sc90) has provided a great deal of data on the relevant cross sections. It turns out that the yield, Y , of giant resonance neutrons at energies above approximately $2k_o$ is nearly independent of energy and nearly proportional to the beam power.

This process may be thought of as one in which the target nucleus is excited by the electron and then decays somewhat later by means of neutron emission. It is a (γ, n) nuclear reaction, written in the scheme of notation in which the first symbol in the parentheses represents the incoming particle in a reaction while the second represents the outgoing particle. In this process the directionality of the incident electron or photon is lost so that these emissions are isotropic. Because of this isotropicity, the inverse square law may be used to estimate the flux density at any given distance r . The spectrum of neutrons of energy E_n is similar to that seen in a fission neutron spectrum and can be described as a Maxwellian distribution,

$$\frac{dN}{dE_n} = \frac{E_n}{T^2} \exp(-E_n / T), \quad (3.16)$$

where T is a **nuclear temperature** characteristic of the target nucleus and its excitation energy. T , in energy units, is generally in the range $0.5 < T < 1.5$ MeV. For this distribution, the most probable value of $E_n = T$ and the average value of $E_n = 2T$. This process generally is the dominant one for incident photon kinetic energies $E_o < 150$ MeV. The excitation functions of total neutron yields in various materials are plotted in Fig. 3.. Table 3.1 gives the total yield, Y_n , of giant resonance neutrons per watt of beam

power ($s^{-1}W^{-1}$), the isotropic differential neutron yield, $dY_n/d\Omega$ ($GeV^{-1} sr^{-1}$) per unit of beam energy per electron, and a recommended dose equivalent source term, S_n , ($Sv cm^2 GeV^{-1}$) per unit beam energy per electron to be used as follows,

$$H = \frac{S_n}{r^2} E_0 I, \quad (3.17)$$

where H is the dose equivalent in Sieverts, r is the radial distance from the target in cm, E_0 is in GeV, and I is the total number of beam particles incident (e.g., during some time interval). The agreement with various experiments is quite good according to Schopper et al. (Sc90).

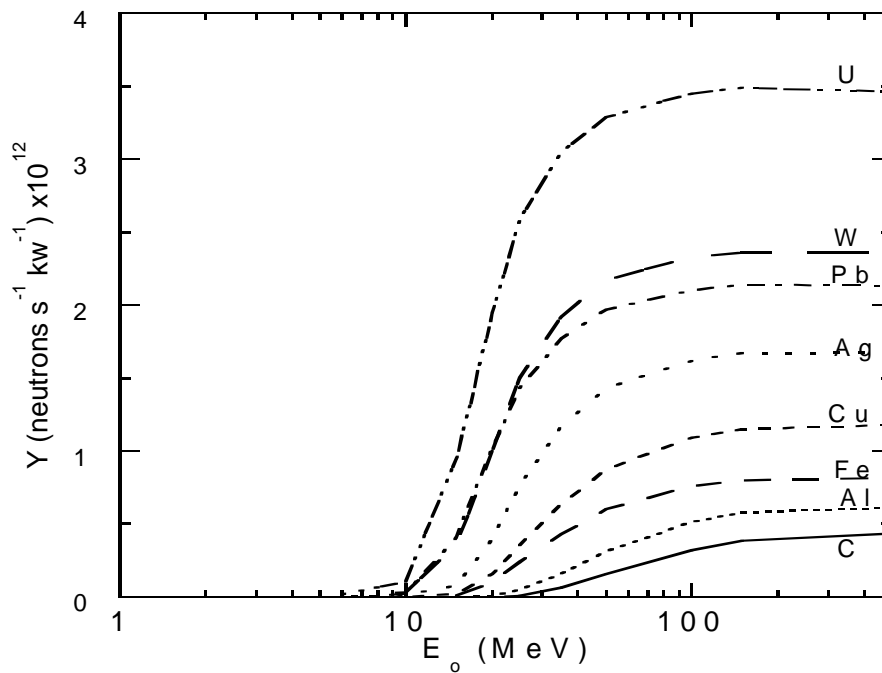


Fig. 3.7 Neutron yields from infinitely thick targets per kW of electron beam power as a function of electron beam energy E_0 , ignoring target self-shielding. [Adapted from (Sw79b).]

Table 3.1 Yields and source terms of giant resonance neutrons in an optimum target geometry per unit beam power (total yield) and per unit incident energy per electron at high energies ($E_o > 500$ MeV). No energy dependence "near threshold" is assumed. [Adapted from (Sw79b) and (Sc90).]

Material	Total Neutron Production Y_n ($s^{-1}W^{-1}$)	Differential Neutron Yield $dY_n/d\Omega$ ($GeV^{-1}sr^{-1}$) per electron	Recommended Source Terms ^a , S_n ($Sv\ cm^2\ GeV^{-1}$) per electron
C	4.4×10^8	5.61×10^{-3}	4.3×10^{-12}
Al ^b	6.2×10^8	7.90×10^{-3}	6.0×10^{-12}
Fe	8.18×10^8	1.04×10^{-2}	7.7×10^{-12}
Ni	7.36×10^8	9.38×10^{-3}	6.9×10^{-12}
Cu	1.18×10^9	1.50×10^{-2}	1.1×10^{-11}
Ag	1.68×10^9	2.14×10^{-2}	1.5×10^{-11}
Ba	1.94×10^9	2.47×10^{-2}	1.8×10^{-11}
Ta	2.08×10^9	2.65×10^{-2}	1.8×10^{-11}
W	2.36×10^9	3.01×10^{-2}	2.0×10^{-11}
Au	2.02×10^9	2.58×10^{-2}	1.8×10^{-11}
Pb	2.14×10^9	2.73×10^{-2}	1.9×10^{-11}
U	3.48×10^9	4.44×10^{-2}	3.0×10^{-11}

^aTo get $Sv\ cm^2\ h^{-1}kW^{-1}$, multiply this column by 2.25×10^{16} .

^bThe value for aluminum is also recommended for concrete.

3.2.4.2 Quasi-Deuteron Neutrons

At energies above the giant resonance, the dominant neutron production mechanism is one in which the photon interacts with a neutron-proton pair within the nucleus rather than with the whole nucleus. The **quasi-deuteron effect** is so-named because for $E_o \approx 30$ MeV the photon wavelength is near resonance with the average inter-nucleon distance so that the photon interactions tend to occur with "pairs" of nucleons. Only neutron-proton pairs have a nonzero electric dipole moment, which makes interactions of photons with such pairs (pseudo-deuterons) favorable. This mechanism is important for $30 < E_o < 300$ MeV and has been described by Swanson (Sw79b). The general effect of this mechanism is to add a tail of higher-energy neutrons to the giant resonance spectrum. For $5 < E_n < E_o/2$ (MeV), the nearly isotropic spectrum of quasi-deuteron neutrons is given by

$$\frac{dN}{dE_n} = E_n^{-\alpha} \text{ where, approximately, } 1.7 < \alpha < 3.6. \quad (3.18)$$

The slope becomes steeper as E_o , the kinetic energy of the incident electron, is approached. Eq. (3.18) is for *thin* targets. For *thick* target situations, the fall-off with E_n is generally steeper. Since the mechanism is the (γ, np) reaction and the neutron and the proton are nearly identical in mass, they share the available energy equally so that the yield of neutrons due this mechanism is essentially zero for neutrons having kinetic

energy $E_n > E_o/2$. In general, the quasi-deuteron neutrons are fewer in number and generally less important than are the giant resonance neutrons. Shielding against the latter will usually provide adequate protection against the former.

3.2.4.3 Neutrons Associated with the Production of Other Particles

There are interactions in which the production of other elementary particles, perhaps best typified by pions, becomes energetically possible at still higher energies ($E_o > 300$ MeV). These particles can then produce neutrons through secondary interactions as will be discussed in Chapter 4. DeStaeblcr (De65) has parameterized the measured yields of high energy particles per incident electron:

$$\frac{d^2Y_n}{dEd\Omega} = \frac{7.5 \times 10^{-4}}{(1 - 0.75 \cos \theta)^2 A^{0.4}} \text{ (GeV}^{-1}\text{sr}^{-1}\text{)}, \quad (3.19)$$

where A is the atomic mass (g mole^{-1}) of the target material. It is reasonable to use a dose equivalent per fluence conversion factor of approximately 1×10^{-13} Sv m^2 (10^{-3} $\mu\text{Sv cm}^2$) for these neutrons.

3.2.5 Muons

With electron beams, muons become of significance above an electron energy of approximately 211 MeV, the threshold of the process in which a μ^\pm pair is produced in a **pair production** process. They can be produced, with much smaller yields, by the decay of π^\pm and K^\pm which are, in turn, due to secondary production processes. Such decay muons will be discussed in Section 4.2.4. A detailed theoretical treatment of muon production by incident electrons is given by Nelson (Ne68 and Ne74). Figure 3.8 gives the muon flux density as a function of electron energy at $\theta = 0^\circ$ while Fig. 3.9 shows an example of the angular dependence of these yields at $E_\mu = 20$ GeV. The reasonableness of scaling with energy to larger values of E_o is well demonstrated.

Obviously, the range-energy relation of muons and considerations related to their energy loss mechanisms discussed in Section 1.4.1 is relevant to shielding against muons regardless of their origin.

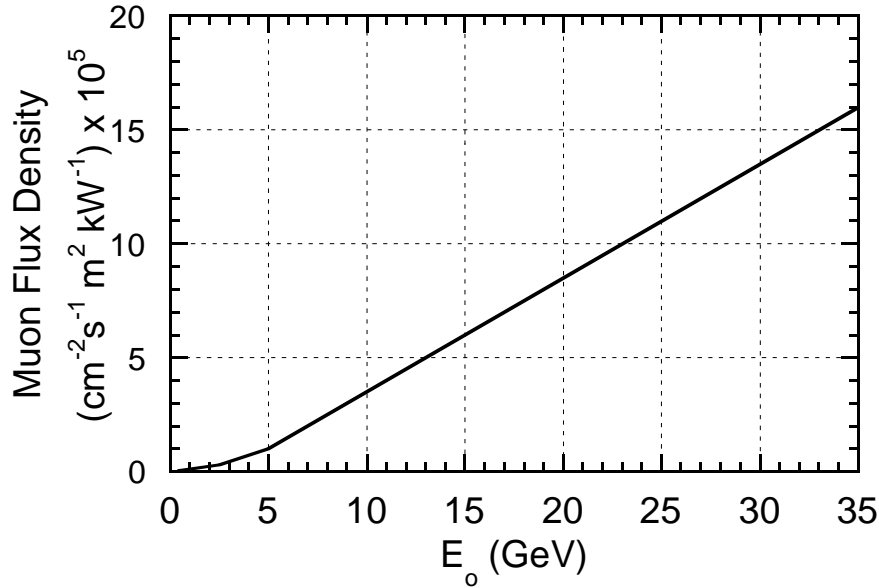


Fig. 3.8 Muon production at $\theta = 0^\circ$ from an unshielded thick iron target at one meter, as a function of electron energy, E_0 . [Adapted from (Ne68a) and (Ne74).]

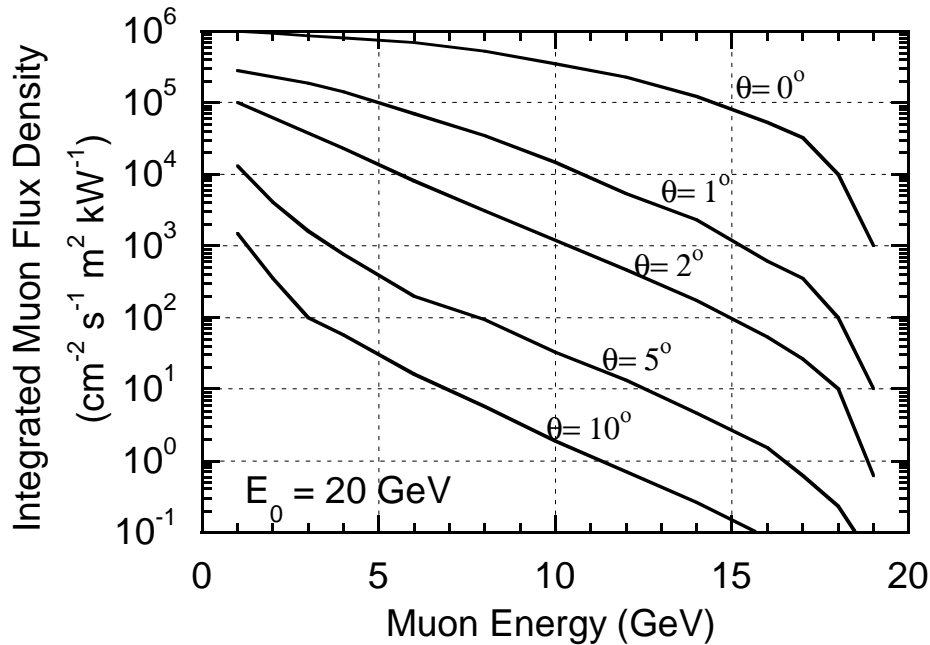


Fig. 3.9 Integrated muon flux density at 1 meter per kW of electron beam power as a function of muon energy for 20 GeV electrons incident on a thick iron target at several values of θ . The integral of the flux density over energy includes all muons that have energies that exceed the value of the abscissa at the specified value of θ . [Adapted from (Ne68a) and (Ne74).]

3.2.6 Summary of Unshielded Radiation Produced by Electron Beams

Swanson (Sw79a) has illustrated the broad features of the radiation field due to the unshielded initial interactions of electrons that is given in Fig. 3.10. This figure is useful for making crude estimates of the resultant radiation field. As one can see, at large angles, from the standpoint of dose equivalent, the unshielded field is always dominated by photons. At small angles, the field is dominated by photons at the lower energies with muons increasing in importance as the energy increases to large values. The production of induced radioactivity will be discussed in Chapters 7 and 8.

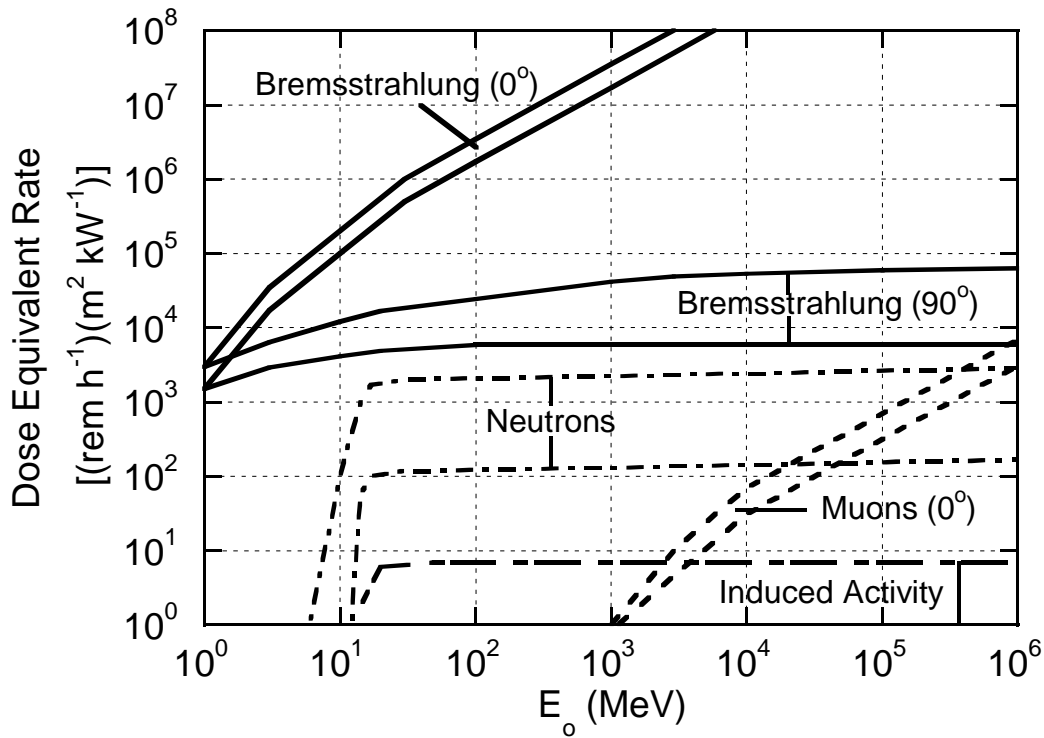


Fig. 3.10 Dose-equivalent rates per unit primary beam power at one meter produced by various types of "secondary" radiations from a high-Z target as a function of primary beam energy, if no shielding were present (qualitative). The width of the bands suggests the degree of variation found, depending on such factors as target material and thickness. The angles at which the various processes are most important are indicated. [Adapted from (Sw79a).]

3.3 The Electromagnetic Cascade-Introduction

The major feature that needs to be considered in the shielding design at electron accelerators is the **electromagnetic cascade**. One should recall the definitions of **critical energy**, E_c and **radiation length**, X_o , that were given in Eq. (3.3a,b) and (1.21), respectively. A related parameter of importance for describing the electromagnetic cascade is the **Molière radius**, X_m ;

$$X_m = X_o E_s / E_c \quad (3.20)$$

$$\text{where } E_s = \left(\sqrt{\frac{4\pi}{\alpha}} \right) m_e c^2 = 21.2 \text{ MeV}, \quad (3.21)$$

where α is the fine structure constant of atomic physics (see Table 1.1), and m_e is the mass of the electron. X_m is a good characteristic length for describing radial distributions in electromagnetic showers. Two additional dimensionless scaling variables are commonly introduced to describe electromagnetic shower behavior;

$$t = x/X_o \quad (\text{for distance scaling}) \quad (3.22)$$

$$\text{and } y = E/E_c \quad (\text{for energy scaling}). \quad (3.23)$$

For mixtures of n elements these quantities and the stopping power dE/dx scale according to the elemental fractions by weight, f_i , according to the Particle Data Group (PDG96), as follows:

$$\frac{dE}{dx} = \sum_{i=1}^n f_i \left(\frac{dE}{dx} \right)_i, \quad (3.24)$$

where all stopping powers are expressed as energy loss per unit areal density (e.g., MeV cm² g⁻¹).

Another term employed is that of the so-called **Compton minimum**, which, as the term is generally used, is the energy where the total photon cross section is at a minimum and the **photon mean free path**, λ_γ , is thus a maximum. The use of this term is somewhat inaccurate since the Compton scattering cross section *monotonically* decreases with energy. The minimum value of the total photon cross section always occurs at energies less than E_c and is typically a few MeV. Figures 3.11 and 3.12 give values of the photon mean free path for a variety of materials as a function of energy.

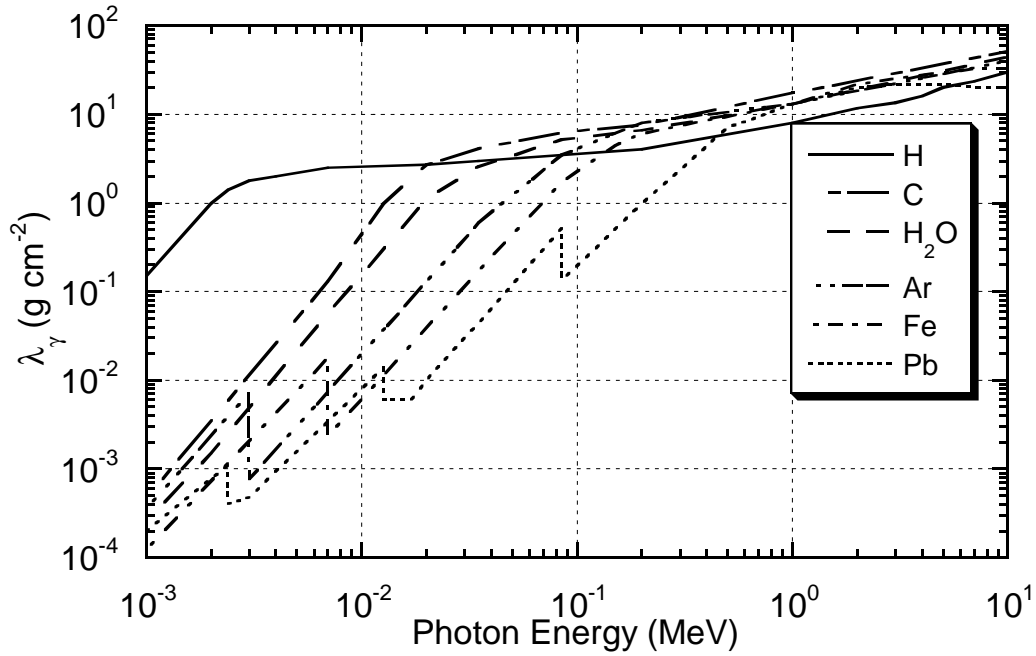


Fig. 3.11 Photon mean free path as a function of photon energy in various materials for low energies. [Adapted from (PDG96).]

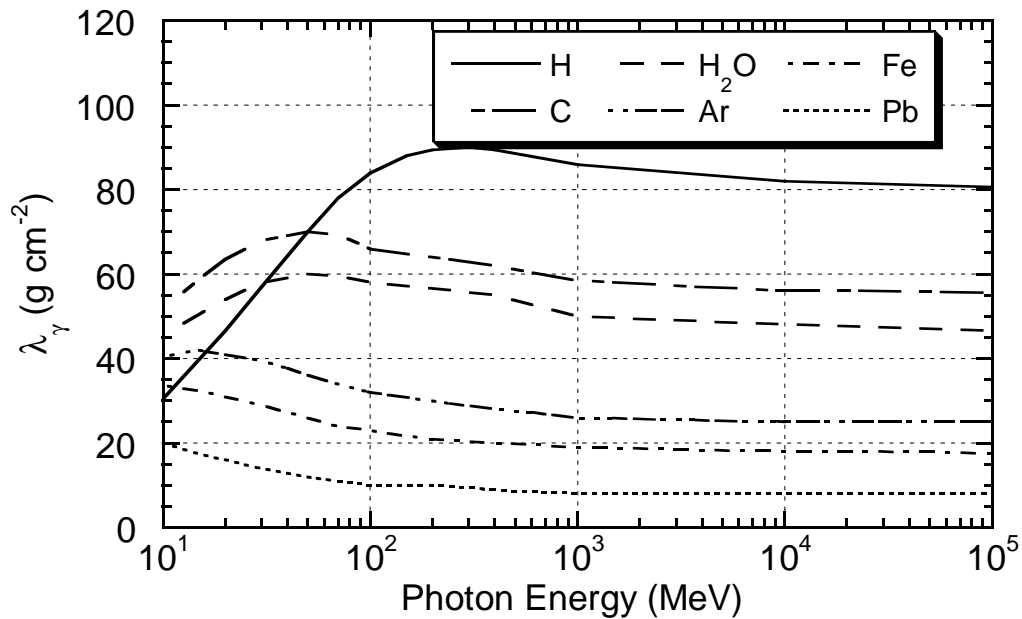


Fig. 3.12 Photon mean free path as a function of photon energy in various materials for high energies. [Adapted from (PDG96).]

For high energy photons ($E_o > 1 \text{ GeV}$), the total e^+e^- pair production cross section, σ_{pair} , is approximately given, for a single element, by

$$\sigma_{pair} = \frac{7}{9} \left(\frac{A}{X_0 N_A} \right) \quad (\text{cm}^2), \quad (3.25)$$

where A is the atomic weight, N_A , is Avogadro's number, and X_o is the radiation length expressed in units of g cm^{-2} . For energies larger than a few MeV, the pair production process dominates the total photon attenuation. The interaction length for pair production, λ_{pair} , is thus given by

$$\lambda_{pair} = \frac{\rho}{N\sigma} (\text{g cm}^2) = \frac{\rho}{A} \frac{7}{9} \left(\frac{A}{X_0 N_A} \right) = \frac{9}{7} X_0. \quad (3.26)$$

The energy-independence and near-equality of λ_{pair} and X_o leads to the most important fact about the electromagnetic cascade:

The electrons radiatively produce photons with almost the same characteristic length for which the photons produce more $e^+ e^-$ pairs.

This is so important because as a first order approximation it means that the "size" in physical space is independent of energy. For **hadronic** cascades, we will later see that the results are considerably different and, one may daresay, more complicated.

Before discussing further the electromagnetic cascade process in detail, one must look a bit more at the dose equivalent due to thick-target bremsstrahlung dose at large values of θ for targets surrounded by cylindrical shields. A picture of the shielding situation is given in Fig. 3.13.

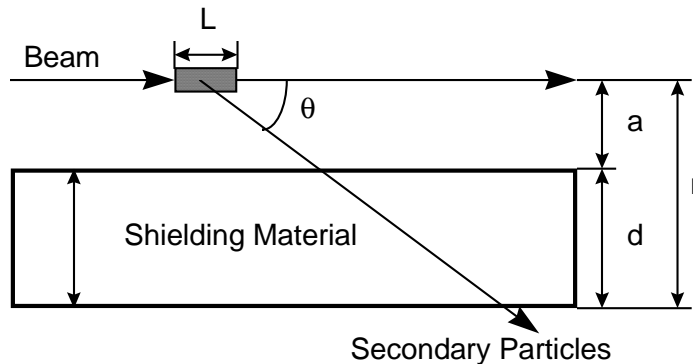


Fig. 3.13 Target and shielding geometry for the estimation of dose equivalent due to electron beam interactions with a target surrounded by a cylindrical shielding. L is the length of the target and the other parameters specify the geometry.

Returning to Eq. (3.8), the results of Swanson and Thomas (Sw90) as improved by Nelson (Ne97) give the photon absorbed dose per incident electron, D , external to such a shield as,

$$D(\theta) = (1 \times 10^{-11}) \left\{ 10.2 E_o \exp(-\theta^{0.6}) + 2.3 \exp(\theta/72) \right\} E_o \left(\frac{\sin \theta}{a+d} \right)^2 \exp\left(-\frac{\mu}{\rho} \frac{\rho d}{\sin \theta} \right) \quad \text{(Gy/electron).} \quad (3.27)$$

As before, this expression is based on results involving iron and copper targets at $E_o = 15$ GeV. Here, E_o is the electron energy in GeV, θ is in degrees, a is the target-to-shield distance (cm), d is the shield thickness (cm), ρ is the shielding material density (g cm^{-3}), and μ/ρ is the attenuation coefficient equal to the value at the ‘‘Compton minimum’’ which for concrete is $2.4 \times 10^{-2} \text{ cm}^2 \text{ g}^{-1}$. The formula implicitly assumes a dose equivalent per unit fluence appropriate at the shower maximum. As a check, for conditions of no shielding present ($d = 0$), the values are within factors of 2 to 5 of those obtained using Eq. (3.9, 3.10, and 3.11). Equipped with this useful parameterization, we shall now proceed to further discussion of the details of development of the electromagnetic cascade.

3.4 The Electromagnetic Cascade Process

Figure 3.14 schematically conceptually illustrates the electromagnetic cascade process.

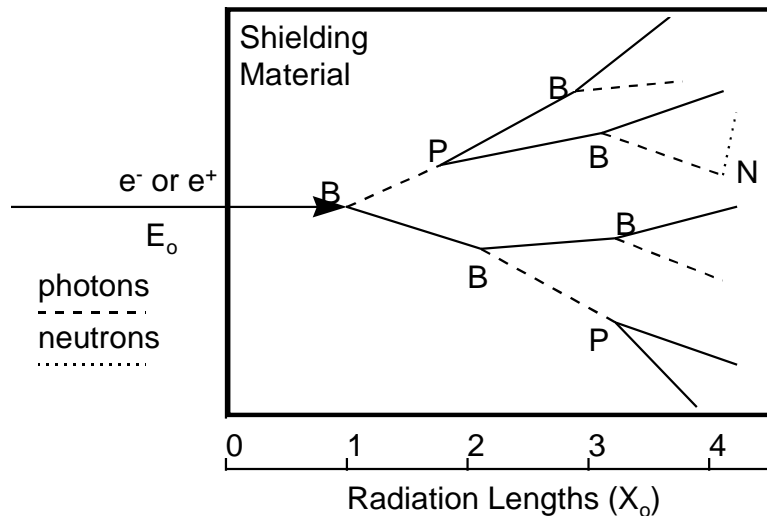


Fig. 3.14 Conceptual view of the development of an electromagnetic cascade in a semi-infinite medium. The solid lines represent electrons or positrons, the dashed lines represent photons, and the dotted lines represent neutrons. The shower is initiated by an electron or positron of energy E_o incident on the medium from the left. The spreading in the transverse direction is greatly exaggerated for clarity. Bremsstrahlung and pair production events are denoted by B and P , respectively. Compton scattering and ionization are both not shown but also play a roles in the dispersal of energy. Photonuclear reactions, as illustrated by the (γ, n) reaction at point N also play a role, albeit much more infrequently than inferred from this illustration. The process could just as well be initiated by a photon. [Adapted from (Sw79a).]

In the simplest terms, the electromagnetic cascade at an electron accelerator proceeds qualitatively according to the following steps:

1. A high energy electron ($E_o \gg m_e c^2$) produces a high energy photon by means of bremsstrahlung.
2. This photon produces an $e^+ e^-$ pair after traveling, on average, a distance of $\frac{1}{3} X_o$. Each member of the pair will have, on average, half the energy of the photon.
3. After traveling an average distance of X_o , each member of the $e^+ e^-$ pair will produce yet another bremsstrahlung photon.
4. Each electron or positron may continue on to interact again and release yet more photons before its energy is totally absorbed.

This chain of events can equally well be initiated by a high energy photon, even one produced in secondary interactions at a hadron accelerator. Eventually, after a number of generations, the individual energies of the electrons and positrons will be degraded to values below E_c so that ionization processes then begin to dominate and terminate the shower. Likewise, the photon energies eventually are degraded so that Compton scattering and the photoelectric effect compete with the further production of $e^+ e^-$ pairs.

Of course, there are subtleties representing many different physical processes, such as the production of other particles, which must be taken into account and are best handled by Monte Carlo calculations. A general discussion of the use of Monte Carlo techniques for such problems has been given by Rogers and Bielajew (Ro90). The most widely-used code incorporating the Monte Carlo method applied to electromagnetic cascades is **EGS** (electron gamma shower), which was written by W. R. Nelson and described by Nelson et al. (Ne85, Ne90) (see Appendix A). Van Ginneken has also written a Monte Carlo program called **AEGIS** (Va78), which is very effective for calculating the propagation of such cascades through thick shields. Analytical approximations have been developed and are summarized elsewhere [e.g., (Sw79a, Sc90)]. The results of published calculations are used in the following discussion to aid in improving the reader's understanding of electromagnetic cascades.

3.4.1 Longitudinal Shower Development

The dosimetric properties of the calculations of an electromagnetic cascade may be summarized in curves that give fluence, dose, or other quantities of interest as functions of shower depth or distance from the axis. Figure 3.15 shows the fraction of total energy deposited (integrated over all radii about the shower axis) versus depth from Van Ginneken and Awschalom (Va75). These authors identified a scaling parameter, ζ , given by:

$$\zeta = 325(\ln Z)^{-1.73} \ln E_0 \quad (\text{g cm}^{-2}), \quad (3.28)$$

where E_0 is in MeV. When longitudinal coordinates are expressed in units of ζ , all curves approximately merge into this universal one and are rather independent of target material.

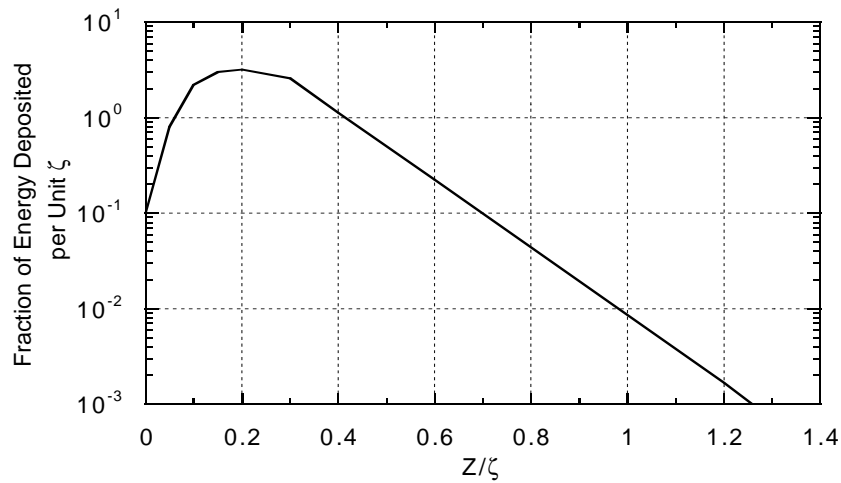


Fig. 3.15 Fraction of total energy deposited by an electromagnetic cascade versus depth integrated over all radii about the shower axis. See Eq. (3.28). [Adapted from (Va75).]

Rossi and Griesen (Ro41), in their epic development of analytical shower theory, have, using their so-called **Approximation B**, predicted for an electron-initiated shower that the total number of electrons and positrons at the shower maximum, N_{show} are proportional to the primary energy as follows:

$$N_{show} = \frac{0.31 E_0 / E_c}{\sqrt{\ln(E_0 / E_c) - 0.37}}. \quad (3.29)$$

This is intuitively sensible as the final outcome of the shower is to divide the energy at maximum among a number of particles with energies near E_c . For a photon-initiated shower, the constant of 0.37 in the denominator becomes 0.18. One can obtain the maximum energy deposited per radiation length from Eq. (3.29) as the product $E_c N_{show}$ (Sc90).

Also from the Rossi/Griesen Approximation B, the location of the shower maximum X_{max} , (along the longitudinal axis usually represented by the z -coordinate) should be given by:

$$\frac{X_{max}}{X_o} = \ln\left(\frac{E_o}{E_c}\right) - C, \quad \text{with } C = 1. \quad (3.30)$$

Experimentally, Bathow et al. (Ba67) found that values of $C = 0.77$ for copper and $C = 0.47$ for lead fit data better. Also, photon-induced showers penetrate about 0.8 radiation lengths deeper than do the electron-induced showers. Schopper et al. (Sc90) simply give values of $C = 1$ and $C = 0.5$ for electron- and photon-initiated showers, respectively. The maximum energy deposited per radiation length is simply given by multiplying N_{show} by the critical energy, E_c .

There are other differences between photon and electron-induced showers but these can normally be neglected. Schopper et al (Sc90) gives the mean squared *longitudinal* spread, τ^2 , (mean square distance lateral spread of the shower about $t \approx t_{max} = X_{max}/X_o$);

$$\tau^2 = 1.61 \ln\left(\frac{E_o}{E_c}\right) - 0.2 \quad \text{(electron-induced shower), and} \quad (3.31)$$

$$\tau^2 = 1.61 \ln\left(\frac{E_o}{E_c}\right) + 0.9 \quad \text{(photon-induced shower).} \quad (3.32)$$

EGS4 results tabulated by Schopper et al. (Sc90) have been parameterized to determine **source terms**, S_i , for longitudinal distributions of absorbed dose in various materials and for the associated dose equivalent within shields comprised of these materials over the energy region of $1 \text{ GeV} < E_o < 1 \text{ TeV}$. This has been done for the dose on the z - axis (subscripts " a ") and for the dose averaged over a 15 cm radius about the z -axis (subscripts " 15 "). Table 3.2 gives parameters for calculating dose equivalent, H_{long} (Sv per electron), at the end of a beam dump of length, L (cm), of density ρ (g cm^{-3}), and gives fitted values of the various "attenuation lengths", λ_i (g cm^{-2}) to be used with the corresponding tabulated values of S_i . For absorbed dose calculations, the factor C , which is the ratio of dose equivalent in tissue (Sv) to absorbed dose in the material (not tissue) (Gy), should be set to unity. The formula in which these parameters from Table 3.2 are to be used is as follows:

$$H_{long} = CS_i \exp(-\rho L / \lambda_i). \quad (3.33)$$

This equation is valid in the longitudinal region beyond the shower maximum.

Table 3.2 Source terms S_a and S_{I5} , and corresponding recommended longitudinal attenuation lengths, λ_a and λ_{I5} , for doses on the axis and averaged over a radius of 15 cm in the forward direction for dumps and end-stops. These results are most valid in the region of incident electron energy, E_o , from 1 GeV to 1 TeV. Conversion factors C from absorbed dose in the shielding material to dose equivalent within the shield are given. E_o is the beam kinetic energy in GeV. These parameters are to be used with Eq. (3.33). [Adapted from (Sc90).]

Material	C (Sv/Gy)	S_a (Gy/electron)	λ_a (g cm ⁻²)	S_{I5} (Gy/electron)	λ_{I5} (g cm ⁻²)
Water	0.95	$1.9 \times 10^{-10} E_o^{2.0}$	58	$1.5 \times 10^{-11} E_o^{2.0}$	59.9
Concrete	1.2	$1.9 \times 10^{-9} E_o^{1.8}$	44	$2.2 \times 10^{-11} E_o^{1.8}$	45.6
Aluminum	1.2	$2.3 \times 10^{-9} E_o^{1.7}$	46	$3.4 \times 10^{-11} E_o^{1.7}$	46.3
Iron	1.3	$2.9 \times 10^{-8} E_o^{1.7}$	30	$1.8 \times 10^{-10} E_o^{1.7}$	33.6
Lead	1.8	$1.9 \times 10^{-7} E_o^{1.4}$	18	$4.6 \times 10^{-10} E_o^{1.4}$	24.2

3.4.2 Lateral Shower Development

Figure 3.16 shows the fraction U/E_o of the incident electron energy that escapes laterally from an infinitely long cylinder as a function of cylinder radius, R , for showers caused by electrons of various energies that bombard the front face of the cylinder. On this graph R is in units of X_m . According to Neal et al. (Ne68b), a function that fits data between 100 MeV and 20 GeV for electrons incident on targets ranging from aluminum to lead is given by

$$\frac{U(R / X_m)}{E_o} = 0.8 \exp[-3.45(R / X_m)] + 0.2 \exp[-0.889(R / X_m)]. \quad (3.34)$$

Results similar to this universal curve have been obtained using EGS4 (Sc90). For values of R/X_m greater than about four, a material-dependent phenomenon emerges in which the photons having the largest mean free paths determined by the photon cross section at the Compton minimum will dominate the slopes of these curves. These extrapolations, normalized to X_m , are also included in this figure. As was done for the longitudinal situation, EGS4 (Sc90) has been similarly used to give the maximum energy deposition (and by extension, the maximum absorbed dose and dose equivalent) as a function of radius R . Over the energy range $1 \text{ GeV} < E_o < 1 \text{ TeV}$, there is direct scaling with energy in the formula for maximum dose equivalent at $\theta \approx 90^\circ$;

$$H_{lat} = CE_o S_{lat} \frac{\exp(-\rho d / \lambda_{lat})}{r^2}, \quad (3.35)$$

where H_{lat} is the maximum dose equivalent laterally (Sv per electron), C is the same as in Eq. (3.33), E_o is the electron kinetic energy in GeV, S_{lat} is the source term from the EGS4 calculations (see Table 3.3), d is the lateral dimension of the shield (shield thickness) in cm, ρ is the density (g cm^{-3}), λ_{lat} is the attenuation length (g cm^{-2}), and r is the distance from the axis, in cm, where the dose equivalent is desired (see Fig. 3.13). Table 3.3 gives the parameters needed for Eq (3.35).

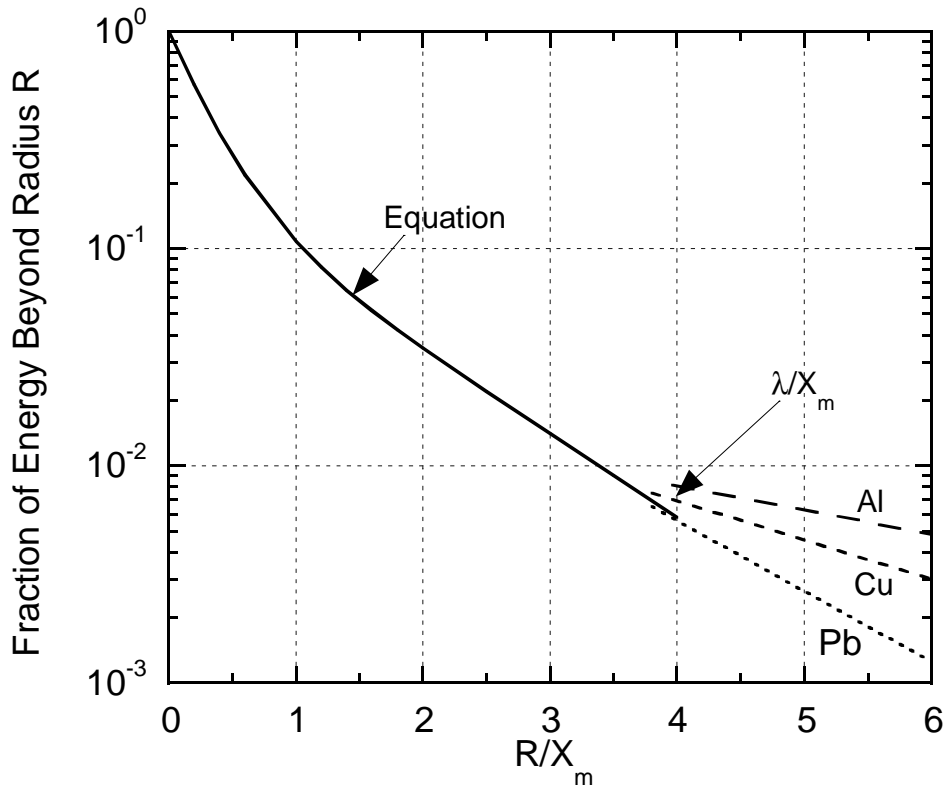


Fig. 3.16 Fraction of total energy deposited beyond a cylindrical radius, R/X_m , as a function of radius, R , for showers caused by 0.1 to 20 GeV electrons incident on various materials. The curve labeled “Equation” refers to Eq. (3.34). [Adapted from (Ne68b).]

Table 3.3 Conversion factors C from absorbed dose in shielding material to dose equivalent, source terms S_{lat} for the maximum of the electromagnetic component, and recommended lateral attenuation lengths λ_{lat} for the electron energy range, E_o , from 1 GeV to 1 TeV laterally for dumps or end-stops. These parameters are to be used with Eq. (3.35). [Adapted from (Sc90).]

Material	C (Sv/Gy)	S_{lat} (Gy cm ² GeV ⁻¹ per electron)	λ_{lat} (g cm ⁻²)
Water	0.95	2.5×10^{-12}	26
Concrete	1.2	3.6×10^{-12}	27
Aluminum	1.2	3.4×10^{-12}	29
Iron	1.3	4.7×10^{-11}	33
Lead	1.8	1.3×10^{-10}	26

3.5. Shielding of Hadrons Produced by the Electromagnetic Cascade.

3.5.1 Neutrons

As discussed before, neutrons are produced by high energy electrons and photons. These neutrons must be taken into account to properly shield electron accelerators. Tesch has summarized shielding against these neutrons by developing simple analytical relations for cases where thick targets are struck by the electron beam (Te88). Figure 3.13 defines the shielding geometry. For lateral concrete shielding, the maximum dose equivalent outside of shield thickness (implying $\theta = 90^\circ$ as defined in Fig. 3.13), d (cm), which begins at radius a (cm) from a thick iron or copper target struck by electrons having primary energy E_o (GeV) is, per incident electron,

$$H(d, a) = \frac{4 \times 10^{-13}}{[(a + d)]^2} E_o \exp(-\rho d / 100) \quad (\text{Sv}). \quad (3.36)$$

This equation is valid for $E_o > 0.4$ GeV and $\rho d > 200$ g cm⁻². For other target materials one can scale this equation in the following way. The neutron production is proportional to the photoproduction cross section, the track length in cm, and the number of atoms cm⁻³. The interaction cross section is generally proportional to the atomic weight A . Since the track length is proportional to X_o ; the production becomes proportional to the radiation length in units of g cm⁻². Thus one can, for rough estimates of dose equivalent in the environs of targets of materials other than iron, obtain results by scaling this value for iron by the factor f ,

$$f = \frac{X_0(\text{material})}{X_0(\text{iron})}. \quad (3.37)$$

For shields comprised of other materials, one can simply adjust the attenuation length (g cm^{-2}), i.e., the value of 100 g cm^{-2} in the exponential function, to that appropriate to the material.

Schopper et al. (Sc90) gives a somewhat more detailed treatment separately handling the giant resonance neutrons and high energy particle components of dose equivalent while deriving "source terms" and appropriate formulas. As above, the geometry for using the formulas given here is defined in Fig. 3.13. The formulae given below are held to be valid for $1 \text{ GeV} < E_o < 1 \text{ TeV}$ and for $30 < \theta < 120$ degrees.

For the giant resonance neutrons, per incident electron,

$$H_n = \eta_n S_n E_o \left(\frac{\sin \theta}{a + d} \right)^2 \exp \left(- \frac{\rho d}{\lambda_n \sin \theta} \right), \quad (\text{Sv}) \quad (3.38)$$

where E_o is the beam energy (GeV), ρ (g cm^{-3}) is the density in, a (cm) and d (cm) are as defined in Fig. 3.13. S_n is the source term from Table 3.1 ($\text{Sv cm}^2 \text{ GeV}^{-1}$), and λ_n (g cm^{-2}) is the attenuation length recommended for giant resonance neutrons listed in Table 3.4. Values of λ_n are given as follows for representative materials. This formula is regarded as being valid for $30 < \theta < 120$ degrees.

Table 3.4 Recommended attenuation lengths for use in Eq. (3.38) for various materials [Adapted from (Sc90).]

Material	λ_n (g cm^{-2})
water	9
concrete	42
iron	130
lead	235

The factor η_n ($\eta_n \leq 1$) is dimensionless and gives an estimate of the efficiency for the production of neutrons by the target. For "conservative" calculations, it can be taken to have a value of unity. It smoothly increases from very small values to unity as the target thickness approaches X_o .

3.5.2 High Energy Particles

In this situation no correction for target thickness is generally employed. This formula uses the same source term as Eq (3.19), per incident electron,

$$H_h = \frac{7.5 \times 10^{-13} E_o}{(1 - 0.75 \cos \theta)^2 A^{0.4}} \left[\frac{\sin \theta}{a + d} \right]^2 \exp \left[- \frac{\rho d}{\lambda_h \sin \theta} \right]. \quad (3.39)$$

Chapter 3 Prompt Radiation Fields Due to Electrons

In this formula H_h is the dose equivalent due to these particles (Sv), E_o is the beam energy (GeV), A is the atomic weight of the target and λ_h (g cm^{-2}) is the attenuation length typical of these particles. The tunnel dimensions a (cm) and d (cm) are defined as before. Table 3.5 gives values of λ_h for representative materials. Schopper et al. (Sc90) goes further and describes a variety of special cases.

Table 3.5 Attenuation lengths λ_h in g cm^{-2} for the high energy particle component. [Adapted from (Sc90).]

Material	Energy Limit > 14 MeV or > 25 MeV (g cm^{-2})	Energy Limit > 100 MeV	Nuclear Interaction Length (g cm^{-2})	Recommended λ_h [Eq. (3.39)] (g cm^{-2})
Water			84.9	86
Aluminum			106.4	128
Soil (sand)	101...104*	117	99.2	117
	102...105 ⁺	96		
Concrete	101...105*	120	99.9	117
	91	105		
	82...100 ⁺	100		
Iron	139 ⁺		131.9	164
Lead	244 ⁺		194	253

*Attenuation lengths for the indicated values are slightly dependent on angle with the higher value at $\theta = 0^\circ$ and the smaller value in the backward direction for $E > 15$ MeV.

⁺Same remark but for $E > 25$ MeV.

Problems

1. An electron accelerator has a beam profile in the form of a 2 mm diameter circle uniformly illuminated by the beam. Make a crude plot of the value of the dose equivalent rate in the beam as the energy increases from 1 MeV to 10 GeV. The average beam current is 1 microamp (1 μA). Assume the beam profile is unchanged during acceleration. Compare with Swanson's simple formula ("conservative" value). Is his formula "conservative" above 100 MeV? (Hint: use Fig. 1.4.)
2. Calculate the critical energy and length of material that corresponds to the radiation length for carbon and for lead. What does this say about the effectiveness of low-Z versus high-Z shielding materials for electrons?
3. A 100 MeV electron accelerator produces a 1.0 μA beam incident on a high-Z (thick) target. Estimate the bremsstrahlung absorbed dose rates at $\theta = 0^\circ$ and 90° at $r = 2$ m from the target using Swanson's rules of thumb. Compare the 0° result with the "in-the-beam dose equivalent rate" found in problem 1. How do the bremsstrahlung and in-beam dose rates compare?
4. Suppose the Tevatron enclosure at Fermilab is converted into an enclosure for an electron synchrotron. The radius of the synchrotron is 1000 m. If the circulated beam is 10^{12} electron, calculate the median energy of the synchrotron radiation photons for $E_0 = 100$ GeV. Also find θ_c of the "lobe."
5. For the accelerator of problem 3, calculate the neutron flux density at $r = 2$ m at large angles using the values in Table 3.1 for a high-Z (tungsten) target. Also use Table 3.1 to estimate the dose equivalent $r = 2$ m. Check this result by "guessing" the average neutron energy is between 1 and 10 MeV and use the curve in Fig. 1.5. Compare this neutron dose with the Bremsstrahlung dose at large angles obtained in problem 3.
6. For a 20 GeV electron accelerator operating at 1 kW, the electron beam strikes a beam stop made of aluminum or iron. How long (in z) does the beam stop have to be to range out all of the muons for either aluminum or iron based on the mean range? Compare the dose equivalent rates at the immediate downstream ends of each material if 10 % of the muons leak through due to straggling and multiple scattering can be neglected. (Assume the production of muons from Fe is approximately equal to that from Al. Recall the inverse square law.)
7. In the discussion of the longitudinal development of electromagnetic showers, there are two different formulations (Rossi-Greisen, Bathow, and Van Ginneken). Using Van Ginneken's scaling method, calculate the value of ζ (g cm^{-2}) for $E_0 = 1000$ MeV, 10 GeV, and 100 GeV for copper and lead. Determine the number of radiation lengths to which ζ , corresponds for each material at each energy.

8. Compare the results of Van Ginneken for the location of the longitudinal shower maximum with Bathow's result for copper and lead at the three energies given in problem 7. Is the agreement better or worse as the energy increases?
9. A hypothetical electron accelerator operates at either 100 MeV or 10 GeV and delivers a beam current of 1 μA . Using Table 3.2, calculate the dose equivalent rates in both Sv/sec and rem/h at the end of a 300 cm long aluminum beam stop; averaged over a 15 cm radius that are due to bremsstrahlung. (The beam stop is a cylinder much larger than 15 cm in radius.) Then assume that, in order to save space, a high-Z beam stop is substituted. How long of a high-Z beam stop is needed to achieve the same dose rates? (Assume lead is a suitable high-Z material.) Why is the length of high-Z shield different for the 2 energies? In this problem, assume the values in Table 3.2 are valid for energies as low as 0.1 GeV.
10. In the accelerator and beam stop of problem 9, if the radius of the beam stop is 30 cm, what is the maximum dose equivalent rate (Sv s^{-1} and rem h^{-1}) on the lateral surface (at contact at $r = 30$ cm) of the beam stop for both energies, 100 MeV and 10 GeV, and both materials? Again assume approximate validity at 100 MeV of the results.
11. Calculate the dose equivalent rate due to neutrons outside a 1 meter thick concrete shield surrounding a cylindrical tunnel (inner radius 1 meter) in which is located a copper target struck by 1 μA beam of 100 GeV electrons. The geometry should be assumed to be optimized for producing giant resonance photoneutrons and the calculations should be performed at $\theta = 30, 60$ and 90° (Concrete has $\rho = 2.5$ g cm^{-3}). Express the result as Sv s^{-1} and rem h^{-1} . For $\theta = 90^\circ$, use Eq. (3.36) as a check.